

Peculiarities of phases of the WMAP quadrupole

Pavel D. Naselsky

Niels Bohr Institute, Blegdamsvej 17, DK-2100 Copenhagen, Denmark, naselsky@nbi.dk

Oleg V. Verkhodanov

Special Astrophysical Observatory, Nizhnij Arkhyz, Karachaj-Cherkesia, 369167, Russia, vo@sao.ru

We present the analysis on the quadrupole phases of the Internal Linear Combination map, ILC(I) and (III) derived by the *WMAP* team (1 and 3-year data release). This approach allows us to see the global trend of non-Gaussianity of the quadrupoles for the ILC(III) map through phase correlations with the foregrounds. Significant phase correlations is found in between the ILC(III) quadrupole and the *WMAP* foregrounds phases for K-W band: the phases of the ILC(III) quadrupole $\xi_{2,1}$, $\xi_{2,2}$ and those of the foregrounds at K-W bands $\Phi_{2,1}$, $\Phi_{2,2}$ display significant symmetry : $\xi_{2,1} + \Phi_{2,1} \simeq \xi_{2,2} + \Phi_{2,2}$, which is a strong indication that the morphology of the ILC(III) quadrupole is mere reflection of that the foreground quadrupole through coupling. To clarify this issue we exploit the symmetry of the CMB power, which is invariant under permutation of the index $m = 1 \Leftrightarrow 2$. By simple rotation of the ILC(III) phases with the same angle we reach the phases of foreground quadrupole. We discuss possible sources of phase correlation and come to the conclusion that the phases of the ILC(III) quadrupole reflect most likely systematic effects such as changing of the gain factor for the 3-year data release with respect to the 1-year, rather than manifestation of the primordial non-Gaussianity.

Keywords: c

osmology: cosmic microwave background – observations – methods: data analysis

1. Introduction

After the release of the Wilkinson Microwave Anisotropy Probe (*WMAP*) 1-year results (hereafter *WMAP* I) Refs. 1, 2, 3, 4 the issue of non-Gaussianity of the CMB has attracted great attention. In the papers Refs. 5, 6, 7, 8, 9, 10, 11, 12, 13, 14, 15, various kinds of methods have been employed and departure of Gaussianity have been detected. These features can be of primordial origin (Refs. 8, 16) or they could be related to foreground residuals (Refs. 17, 18, 19) or any sort of systematic effects (9).

Recently the *WMAP* team released the 3-year data (hereafter *WMAP* III) Ref. 20 producing Internal Linear Combination map (ILC(III)) available for scientific analysis at the multipole range $\ell \leq 10$. The *WMAP* team performed the analysis of Gaussianity for the ILC(III) signal that does not include harmonics $\ell \leq 10$ and showed that the CMB signal is Gaussian Ref. 21. However, as it was

cautioned by the *WMAP* team, the alignment and planarity at multipoles $\ell = 2, 3$ and 5 mentioned in Refs. 8, 9, 11, 12, 22 still present in the map (see recent investigation in Ref. 23).

If breaking of statistical isotropy in the low multipoles is of primordial origin, a very fundamental issue is consequently raised: what cosmological model can provide such a peculiar structure in the CMB angular distribution on the sky? In Refs. 8, 24 and 25 it has been pointed out that breaking of statistical isotropy in the low multipoles can be explained and in favor of the Bianchi VIII model. However, Helling, Shupp and Tesileanu (Ref. 26) have also pointed out that $\ell = 2, 3$ and 5 have anti-alignment in the direction of non-cosmological dipole and argued that accurate technique of the CMB signal subtraction probably needs to be non-linear (with respect to dipole treatment) to prevent any residuals from the dipole in the map.

In addition, methods of foreground separation for the CMB signal very likely leave foreground residuals in the CMB map, a problem that can be illustrated by cross-correlation between the derived signal and the foregrounds. For the WMAP I data this problem was already investigated in Refs. 27, 28, 17, 18, 29, 30.

For WMAP III data, it has been shown in Refs. 31, 18 that the low multipoles in ILC(III) clearly display significant cross-correlation with the derived foregrounds, while Ref. 32 showed that negative peak at $b = -57^\circ, l = 209^\circ$) has no analogue in the foreground map. In Refs. 33, 10 analyzing the *WMAP* map-making algorithm (MMA) it has been pointed out that it could produce some residuals from the non-cosmological dipole (related with the motion of our Galaxy in the Local Group) and any non-Gaussian features can “naturally” arise as the result of the MMA. Summarizing present status of non-Gaussianity and statistical anisotropy of the CMB for low multipoles $l \leq 10$, we may say that the origin of these peculiarities still is uncertain.

In this paper we go back to the question raised in Refs. 13 and 34, if the *WMAP* quadrupole is cosmological? To answer this question, we will implement the analysis of the ILC(I), ILC(III) and de Oliveira-Costa & Tegmark (Ref. 35) quadrupole and compare their phases with those of the WMAP III foregrounds^a: combined maps from the synchrotron, free-free, dust emission at K-W band. We will show that combination of the ILC(III) phases $\xi_{2,m}$ and the foreground phases $\Phi_{2,m}$ follow the intriguing relation $\xi_{2,m} + \Phi_{2,m} \simeq const$ with accuracy, e.g. within 0.014 (rad) for the foreground at K band. Since phases of the signal is closely related to morphology of the maps (Ref. 36), detected correlation between the ILC(III) and foreground phases allow us to conclude that it is most likely due to systematic effects (such as estimation of the gain factor and foreground separation) rather than primordial one.

^ahttp://lambda.gsfc.nasa.gov/product/map/m_products.cfm

2. Phase analysis of the WMAP data

For the statistical characterization of the CMB temperature anisotropies on a sphere where θ and φ are polar and azimuthal angle of the polar system of coordinate, it is useful to express $\Delta T(\theta, \varphi)$ in terms of spherical harmonics $Y_{\ell m}(\theta, \varphi)$:

$$\Delta T(\theta, \varphi) = \sum_{\ell=0}^{\ell_{\max}} \sum_{m=-\ell}^{\ell} |a_{\ell, m}| \exp(i\phi_{\ell, m}) Y_{\ell m}(\theta, \varphi) \quad (1)$$

where $|a_{\ell, m}|$ and $\phi_{\ell, m}$ are the amplitudes and phases of the coefficients $a_{\ell, m}$, respectively, and $|m| \leq \ell$. $\Delta T(\theta, \varphi)$ can be full-sky signal, such as the WMAP frequency maps from K to W band. We denote for the ILC and the foreground coefficients as $c_{\ell, m} \equiv |c_{\ell, m}| \exp(i\xi_{\ell, m})$ and $F_{\ell, m}^{(j)} \equiv |F_{\ell, m}^{(j)}| \exp(i\Phi_{\ell, m}^{(j)})$, respectively. Here $\xi_{\ell, m}$ and $\Phi_{\ell, m}^{(j)}$ are the corresponding phases and the index $j = 1 - 5$ marks the WMAP frequency band for K, Ka, Q, V and W bands, respectively. In standard cosmological models (i.e. those involving the simplest forms of inflation) these temperature fluctuations constitute a realization of a statistically homogeneous and isotropic Gaussian random field. The statistical properties of Gaussian random fields are completely determined by the power spectrum

$$\langle a_{\ell m} a_{\ell' m'}^* \rangle = C_{\ell} \delta_{\ell \ell'} \delta_{m m'}, \quad (2)$$

where the angle brackets indicate ensemble average. For any single realization of signal, the angular power spectrum is estimated

$$C_{\ell} = \frac{1}{2\ell + 1} \sum_{m=-\ell}^{\ell} |a_{\ell m}|^2. \quad (3)$$

As the signal is always real, the conjugate properties of the spherical harmonic coefficients allow us to write down the angular power spectrum as

$$C(\ell) = \frac{1}{2\ell + 1} |c_{\ell, 0}|^2 + \frac{2}{2\ell + 1} \sum_{m=1}^{\ell} |c_{\ell, m}|^2. \quad (4)$$

2.1. Linear phase correlation method.

To investigate different correlation of phases for different signals (the CMB and foregrounds) we need to implement as much as possible methods to detect corresponding correlations and then to show their possible sources. One of the possible method is to draw different linear combination of the phases in form

$$G_{l, m} = \sum_j \alpha_j \psi_{l, m}^{(j)} \quad (5)$$

where α_j is $(-1, 0, 1)$ and $\psi_{l, m}^{(j)}$ are the phases of different signals j . The basis of this method has simple motivation from the analysis of the non-Gaussian random process recently performed in Refs. 37 and 38. If non-linearity of the random process $\delta(\vec{x})$, which leads to its non-Gaussianity has simple quadratic form, the standard method

of the correlation analysis is the bispectrum. It is defined as Fourier transform of the tree-point correlation function

$$\zeta(\vec{r}_1, \vec{r}_2) = \langle \delta(\vec{x})\delta(\vec{x} + \vec{r}_1)\delta(\vec{x} + \vec{r}_2) \rangle \quad (6)$$

Generally speaking for any non-Gaussian processes we need to know all high order cross-correlations or polyspectra, which are negligible for the Gaussian random process. However, we may characterize this sort of Non-Gaussianity in terms of phase correlation. For process characterized by the bispectrum only, corresponding equation for the phase coupling, which maximizes the bispectrum, has a form (Refs. 37, 38)

$$\mathbf{G}(\vec{k}) = 2\theta_{\vec{k}} - \theta_{2\vec{k}}; \quad \mathbf{G}(\vec{k}, \vec{p}) = \theta_{\vec{k}} + \theta_{\vec{p}} - \theta_{\vec{p}+\vec{k}} \quad (7)$$

where $\theta_{\vec{k}}$ is the Fourier phase of the random process $\delta(\vec{x})$.

As one can see from Eq.(7), linear combination of the phases characterizes non-linear coupling of the modes tested by bispectrum or in general case by polyspectrum. This is the reason why we introduce the functional $\mathbf{G}_{\ell,m}$ to investigate different high order moments of the CMB-foreground cross-correlation.

2.2. Symmetry of the power spectrum.

Let us discuss the properties of the second term in Eq.(4). This part of the power spectrum is invariant under the following transformation $\mathbf{d}_{\ell,m} = \wp \mathbf{c}_{\ell,m'}$, $d_{\ell,m=0} = c_{\ell,m=0}$, where \wp is the permutation operator for $m' \leq \ell$. For the quadrupole component

$$\begin{pmatrix} d_{2,1} \\ d_{2,2} \end{pmatrix} = \begin{pmatrix} 0 & 1 \\ 1 & 0 \end{pmatrix} \begin{pmatrix} c_{2,1} \\ c_{2,2} \end{pmatrix}, \quad (8)$$

i.e. this operator simply exchanges $m = 1$ and 2 without altering the power spectrum $C(\ell)$. However, the map after such implementation of the operator \wp

$$\Delta\bar{T}(\theta, \varphi) = \sum_{\ell=2}^{\ell_{\max}} \sum_{m=-\ell}^{\ell} |d_{\ell,m}| e^{i\Psi_{\ell,m}} Y_{\ell m}(\theta, \varphi) \quad (9)$$

is not invariant. As one can see from Eq.(8), the phases of the $d_{2,m}$ and $c_{2,m}$ coefficients correspond to the following equations: $\Psi_{2,1} = \xi_{2,2}$ and $\Psi_{2,2} = \xi_{2,1}$. What is important is that if $c_{\ell,m}$ constitute a Gaussian random field the phases $\xi_{\ell,m}$ should have no correlation with the foreground phases $\Phi_{\ell,m}$, which should also be the case for the $\Psi_{\ell,m}$ as well. In Fig.1 we plot the ILC(I) quadrupole in galactic coordinates and the corresponding transformed map by the permutation operator \wp , which have the same quadrupole power.

3. Phase analysis of the WMAP first (WMAP I) and third (WMAP III) years the CMB quadrupoles.

Below we examine the phases of the ILC and those of the foregrounds in more detail. Firstly, we plot the phases for the ILC(I) and the foreground and the frequency

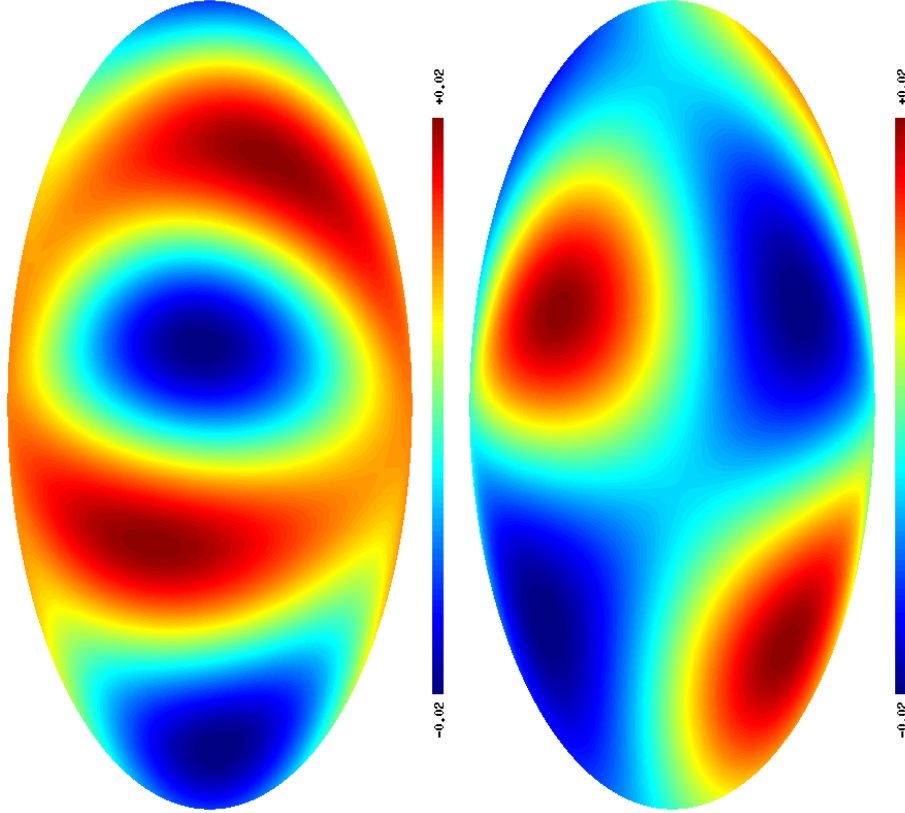


Fig. 1. The map for the ILC(III) quadrupole (top) and the transformed map by the permutation operator φ (bottom). These two maps have the same quadrupole power.

maps from WMAP I in Fig.2. The phases for foregrounds at Q and V band and for frequency map at Q-W to show that $\xi_{2,1} \simeq \Phi_{2,1}^{(3,4)}$ (see errors in the Table 1). For K and Ka foregrounds the correlation are even stronger than for Q band.

As one can see from Table 1, the phase of the ILC(I) $\xi_{2,1}$ is extremely close to the phase of the foreground $\Phi_{2,1}$ while the phase difference $\Phi_{2,2} - \xi_{2,2}$ is close to π . To specify the probability of such realization of the phases from uniformly distributed and non-correlated CMB phases with the foregrounds, we can use two vectors $\vec{n}_1 = (\cos \xi_{2,1}, \sin \xi_{2,1})$ and $\vec{n}_2 = (\cos \xi_{2,2}, \sin \xi_{2,2})$ for the ILC(I) and $\vec{f}_1 = (\cos \Phi_{2,1}, \sin \Phi_{2,1})$ and $\vec{f}_2 = (\cos \Phi_{2,2}, \sin \Phi_{2,2})$ for the foregrounds.

	F^Q	F^V	F^W	Q	V	W
(2, 1)	0.024	0.044	0.291	-0.026	-0.005	0.015
(2, 2)	3.508	3.465	3.479	3.603	3.787	3.940

As is proposed for the multipole vector in Refs. 22, 26, we can characterize the

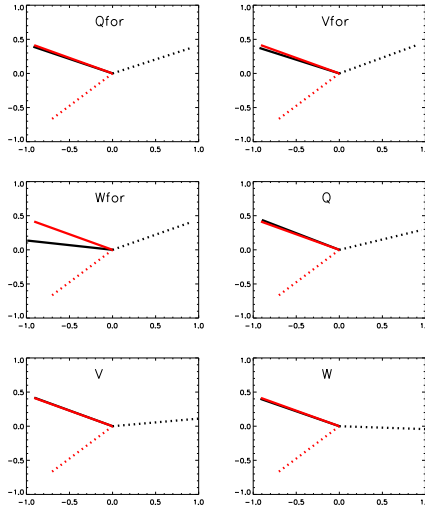


Fig. 2. Phases of the WMAP I, V and W band signals. The phase is represented by the angle subtended between the positive x axis and the line. Solid lines are for $(\ell, m) = (2, 1)$ modes and dotted lines for $(\ell, m) = (2, 2)$. Red lines are the ILC(I) phases and are plotted in all 6 panels whereas black lines are for either foreground maps or frequency maps. Notice the overlapping of phases at the $(2, 1)$ component between the ILC(I) and Q and V foreground maps, and Q, V and W frequency maps. The difference is listed in Table 1.

correlations of these unit vectors in terms of scalar and vector product: $(\vec{n}_i \cdot \vec{f}_i)$ and $(\vec{n}_i \times \vec{f}_i)$. Following Helling, Shupp and Tesilleanu (Ref. ?), we use the vector product for estimation of the probability to get realization with $\vec{n}_1 \times \vec{f}_1 = \sin(\Phi_{2,1} - \xi_{2,1})$ as

$$P(\Phi_{2,1}, \xi_{2,1}) = \frac{1}{2} C_1^2 \sin 2(\Phi_{2,1} - \xi_{2,1}) \quad (10)$$

where $C_p^k = k!/(k-p)!$. Since $\Phi_{2,1} - \xi_{2,1} \ll \pi/2$, this probability corresponds to the phase difference $\Phi_{2,1} - \xi_{2,1}$ multiplied by a factor of 2. From Table 1 one can see that for Q band foreground it is about 5% .

As is claimed by the WMAP science team, improvement of systematic effects, including the gain factor, leads to correction of the foregrounds and the ILC(I) map. We show below that this improvement reveals significant correlations between the ILC(III), the foregrounds and non-cosmological dipole phases. First, we start from analysis of the difference between ILC(III) and ILC(I) map. In Fig.3 we plot the quadrupole map for ILC(III)-ILC(I) in Galactic coordinates.

Correction of the foregrounds in WMAP III and the ILC(III) in comparison with WMAP I leads to the changes of the ILC(III) and the foregrounds phases as shown in Fig.4. In Table 2 we list the phase differences for $\Phi_{2,1} - \Phi_{2,2}$ and $\xi_{2,2} - \xi_{2,1}$. As one can see from Fig4, the phases of ILC(III) now are significantly different with respect to the ILC(I), while the phases of quadrupole for the foregrounds at $(2, 2)$ are still shifted by $\sim \pi$. The bottom right panel marked with ‘‘DIP’’ in Fig4 shows the shift

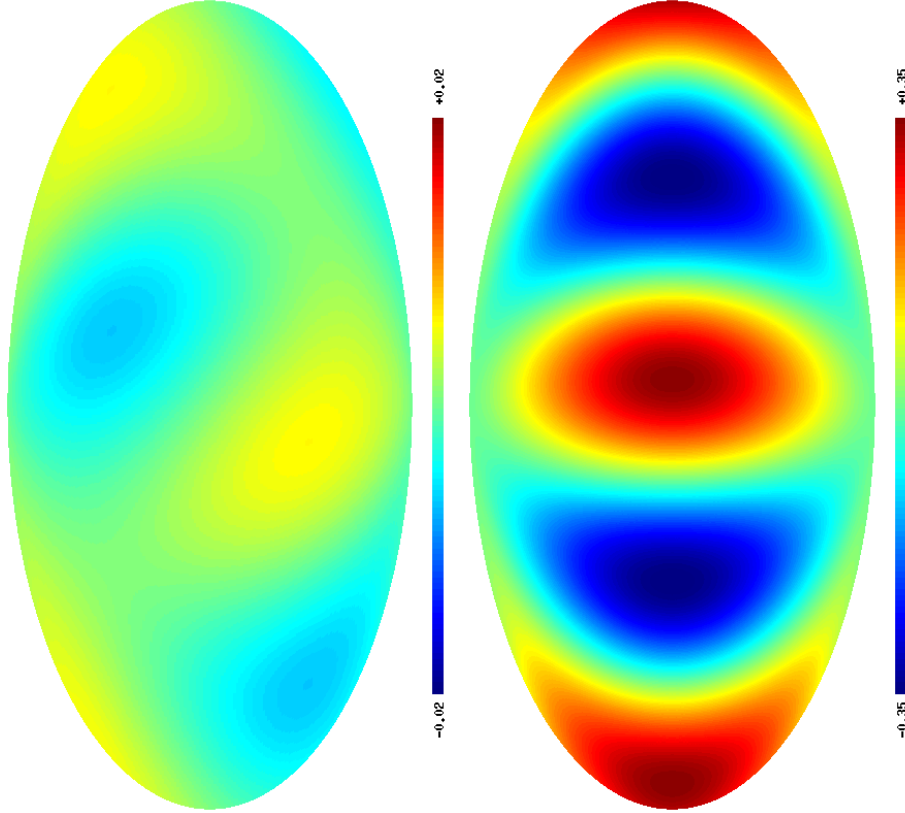


Fig. 3. The map for difference between the ILC(III) and ILC(I) (top) and that for difference between the K band foreground WMAP III and WMAP I (bottom).

of phases for the ILC(III) quadrupole with respect to both non-cosmological and cosmological dipole phase $((\ell, m) = (1, 1))$ from ILC(III).

From K and Ka band of the Table 2 one can write down an empirical equation

$$\begin{aligned}
 \xi_{2,1} + \Phi_{2,1} &\simeq \xi_{2,2} + \Phi_{2,2} = 4.46963(-0.0147) \quad ; \text{K} \\
 \xi_{2,1} + \Phi_{2,1} &\simeq \xi_{2,2} + \Phi_{2,2} = 4.42253(+0.0396) \quad ; \text{Ka}
 \end{aligned}
 \tag{11}$$

	F^K	F^{Ka}	F^{Q}	F^{V}	F^{W}
$\Phi_{2,1}^{(i)} - \Phi_{2,2}^{(i)}$	2.4916	2.4373	2.3886	2.2974	2.3557
$(\xi_{2,2} - \xi_{2,1}) - (\Phi_{2,1}^{(i)} - \Phi_{2,2}^{(i)})$	0.0147	0.0396	0.0881	0.2471	0.1211

The probability for the phases of the foregrounds and the non-correlated phases

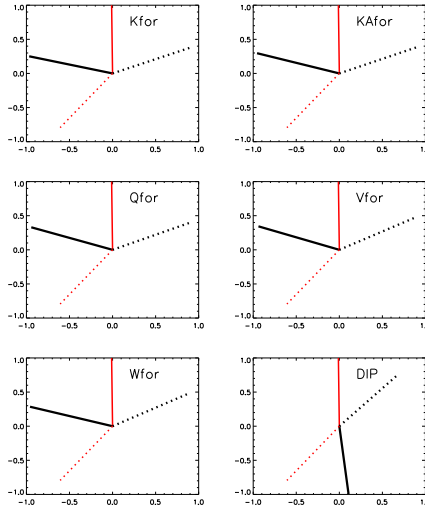


Fig. 4. Phases of WMAP III foregrounds and the ILC(III). The phase is represented by the angle subtended between the positive x axis and the line. Solid lines are for $(\ell, m) = (2, 1)$ modes and dotted lines for $(\ell, m) = (2, 2)$. Black lines are for foregrounds and red lines are for ILC(III). The bottom right panel shows the ILC(III) phases in red, the non-cosmological dipole $((\ell, m) = (1, 1))$ phase (black solid line) and the cosmological dipole one (black dotted line).

to satisfy Eq.(11) is exactly the modulo of difference between $\xi_{2,1} + \Phi_{2,1}$ and $\xi_{2,2} + \Phi_{2,2}$, as shown in the brackets in Eq.(11).

Correlation of phases in the form of Eq.(11) can be easily explained in terms of phase correlation after the permutation operation on the phases. Taking account of $\Psi_{2,1} = \xi_{2,2}$ and $\Psi_{2,2} = \xi_{2,1}$, from Eq.(11) we obtain $\Psi_{2,1} - \Phi_{2,1} \simeq \Psi_{2,2} - \Phi_{2,2}$ and rotation of the $d_{2,m}$ phases by the angle $\Delta = \Psi_{2,1} - \Phi_{2,1}$ transforms the phases $\Psi_{2,1} - \Delta, \Psi_{2,2} - \Delta$ to the phases of the foregrounds $\Phi_{2,1}, \Phi_{2,2}$.

As is shown in Table 2, the probability for ILC and foreground phases to follow Eq.(11) for uniformly distributed and statistically independent from the foregrounds Gaussian CMB signal increase from ~ 0.09 for Q band and reach the maximum 0.22 for the V band and falls down to 0.12 for the W band. This result seems to have natural explanation, since the contribution of the synchrotron emission to the Q, V and W bands decrease, and the free-free and dust emission dominate over synchrotron emission.

4. Multipole vectors analysis

In this section we compare the phase correlation method with multipole vectors approach, proposed in Refs. 13, 23. We apply the multipole vectors method for the ILC(III) quadrupole and kinetic quadrupole. After this we calculate the multipole vectors using the method in Ref. 23.

The values of ILC quadrupole $a_{\ell m}$ are:

$$\begin{array}{rcc}
 \ell & m & \Re & \Im \\
 2 & 0 & +1.147576980 \times 10^{-2} & 0 \\
 2 & 1 & -5.329925261 \times 10^{-5} & +4.864335060 \times 10^{-3} \\
 2 & 2 & -1.440715604 \times 10^{-2} & -1.880360022 \times 10^{-2}
 \end{array}$$

After correction of the kinetic quadrupole, we have

$$\begin{array}{rcc}
 \ell & m & \Re & \Im \\
 2 & 0 & +1.147431601 \times 10^{-2} & 0 \\
 2 & 1 & -5.358225098 \times 10^{-5} & +4.866961855 \times 10^{-3} \\
 2 & 2 & -1.440600399 \times 10^{-2} & -1.880334876 \times 10^{-2}
 \end{array}$$

According to Ref. 13 we describe these $a_{\ell m}$ by multipole vector with coordinates $(-0.562380, 0.815276, 0.138036)$ and $(0.970920, 0.048491, 0.234440)$ which correspond to the points on a sphere with Galactic coordinates (in degrees) $(l = 124.6, b = 7.9)$ and $(l = 2.9, b = 13.6)$ respectively.

We perform the same conversion for the K band. The input data are

$$\begin{array}{rcc}
 \ell & m & \Re & \Im \\
 2 & 0 & -2.167431593 \times 10^{+0} & 0 \\
 2 & 1 & -1.421663761 \times 10^{-1} & 4.126564786 \times 10^{-2} \\
 2 & 2 & +4.031517506 \times 10^{-1} & 1.558263451 \times 10^{-1}
 \end{array}$$

After correction for the kinetic quadrupole, we have

$$\begin{array}{rcc}
 \ell & m & \Re & \Im \\
 2 & 0 & -2.167433023 \times 10^{+0} & 0 \\
 2 & 1 & -1.421666592 \times 10^{-1} & 4.126827419 \times 10^{-2} \\
 2 & 2 & +4.031529129 \times 10^{-1} & 1.558265984 \times 10^{-1}
 \end{array}$$

This gives us the corresponding multipole vector coordinates and the Galactic positions on a sphere: $(-0.560275, 0.076989, 0.824721)$, $(l = 172.2, b = 55.6)$ and $(-0.479820, 0.113498, -0.869995)$, $(l = 166.7, b = -60.5)$.

Using statistics for such vectors, we have found area vectors in a form

$$w^{(2;1,2)} = v^{(2,1)} \times v^{(2,2)}. \quad (12)$$

This gives us the area vectors with coordinates w_{III} : $(0.1850, 0.2657, -0.2194)$ or $(l = 55.2, b = -34.1)$ and w_K : $(-0.1602, -0.8826, 0.0033)$ or $(l = 259.7, b = 0.2)$.

After this we calculated statistics following Ref. 23 to estimate correlation properties: dot product of ILC and K-channel vectors

$$d^{(2,i)} = v_{III}^{(2,i)} \cdot v_K^{(2,i)}, \quad (13)$$

dot product of ILC and K-channel area vectors

$$\Delta^{(2;1,2)} = \frac{w_{III}^{(2;1,2)} \cdot w_K^{(2;1,2)}}{|w_{III}^{(2;1,2)}| |w_K^{(2;1,2)}|}, \quad (14)$$

and ratio of lengths

$$r^{(2;1,2)} = \frac{|w_K^{(2;1,2)}|}{|w_{II}^{(2;1,2)}|} \quad (15)$$

So, we have got

$$\begin{aligned} d^{(2,1)} &+0.4908 \\ d^{(2,2)} &-0.6643 \\ \Delta^{(2;1,2)} &-0.7550 \\ r^{(2;1,2)} &+2.2939 \end{aligned}$$

As one can see from this Table, all the dot and cross-products are not especially close to unity (see for comparison Table 2 in Ref. 23 for ILC(I) and ILC(III), for which $d^{(2,1)} \simeq 0.973, d^{(2,2)} \simeq 0.956, \Delta^{(2;1,2)} \simeq 0.955$ and $r^{(2;1,2)} \simeq 0.952$), which means that the multipole vector approach is not very sensitive for analysis of the CMB-foreground correlations.

5. Discussions

5.1. Systematic effects ?

For interpretation of correlations between the *WMAP* low multipoles (i.e. alignment for $\ell = 2, 3$, planarity for $\ell = 5$ etc.) we need to know how possibly systematic effects determine their properties. This problem will be even more crucial if one is to explain the deficit of the ILC quadrupole power. We will need to implement modification of the theory of inflation (cut-off in power for primordial adiabatic fluctuations at spatial scales $> 10^3$ Mpc), the Bianchi VIIIh model, or any theoretical changes of the cosmological scenario, assuming primordial origin of the ILC(III) low amplitude quadrupole.

Probably, the best and more significant illustration of the systematic effects is the improvement of the gain factor performed by the *WMAP* science team, which could be the reason why the quadrupole from ILC(I) has different amplitude and phases in comparison with from ILC(III). More importantly, the quadrupole power of the ILC(I) and the ILC(III) does not change as much as the phases reveal of a new sort of correlation between the ILC(III) phases and the foreground phases (see Eq.(11)). In Fig.5 we plot the corresponding phases for the map of difference between the ILC(III) and the ILC(I) quadrupoles. Next type of systematic effect is illustrated by the comparison of the ILC(III) quadrupole and the quadrupole derived by de Oliveira-Costa and Tegmark (Ref. 35) from the *WMAP* I and the *WMAP* III. Difference between the ILC(III) and de Oliveira-Costa & Tegmark (Ref. 35) quadrupoles is mainly related with different Galactic mask, which we will call M05 and M06 (following Ref. 35). As one can see from Fig.5 and Table 3, the error of the $\xi_{2,1}$ ILC phase reconstruction is about 0.1 radians for M06 and it is negligible for M05 mask. For $\xi_{2,1}$ the corresponding error is ~ 0.12 radians (M06) and ~ 0.05 radians

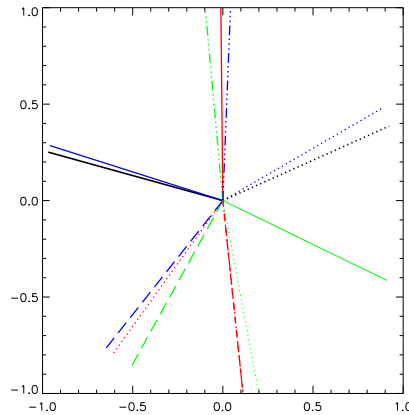


Fig. 5. Phases of WMAP III foregrounds and the ILC(III). The phase is represented by the angle subtended between the positive x axis and the line. Solid lines are for $(\ell, m) = (2, 1)$ modes and dotted lines for $(\ell, m) = (2, 2)$. Red lines are for ILC(III), black and blue lines for K and W band foregrounds, respectively. Green for ILC(III)-ILC(I). Thick red dash line is for non-cosmological dipole. Thick blue and green are for M05 and M06 respectively, in which dash lines and triple dot-dash lines are for $(2, 1)$ and $(2, 2)$, respectively.

	ILC(III)	Δ	M05	M06
$(2, 1)$	1.582	5.856	1.528	1.668
$(2, 2)$	4.059	4.909	4.010	4.181

(M05). This means that with uncertainties about ± 0.12 radians Eq.(11) is correct for all the K-W foregrounds.

Let us discuss another important correlations of the ILC(III) phases and the phases of non-cosmological and “cosmological” dipoles shown in Fig.4. By dipole phase we mean the phase of $(\ell, m) = (1, 1)$ mode. The angle between $\xi_{2,1} = 1.528$ and the non-cosmological dipole $\Psi_{nc} = 4.824$ is about $\alpha = \Psi_{nc} - \xi_{2,1} = 3.295$ radians, while the angle between $\xi_{2,2} = 4.0586$ and the phase of cosmological dipole $\Psi_c = 0.8379$ is $\beta = \xi_{2,2} - \Psi_c = 3.2207$. Thus, $\alpha - \beta \simeq 0.074$ rad for the ILC(III).

We would like to point out that the above-mentioned correlations between the phases of the ILC(III) and those of the WMAP III foregrounds are mainly related to the changes of the gain factor. The crucial part of these correlations is the angle between $\xi_{2,2} - \xi_{2,1}$ and for the foreground phases $\Phi_{2,2} - \Phi_{2,1}$. Note that transition from the WMAP I to WMAP III leads to rotation of the phases for the ILC and for the foregrounds as well. Since WMAP III data seem more accurate in terms of systematic effect removal, decreasing of direct correlations between $\xi_{2,1}$ and $\Phi_{2,1}$, typical for the WMAP I, reveals another type of correlation between the ILC(III)

and the foregrounds. In particular, in addition to Eq.(11) one can get

$$\begin{aligned}\xi_{2,2}^I - \xi_{2,1}^I &\simeq 1.186 \text{ rad.} \\ \xi_{2,1}^I - \xi_{2,1}^{III} &\simeq 1.133 \text{ rad.}\end{aligned}\quad (16)$$

which means that the phases for the ILC(I) and ILC(III) have some regular changes. It is quite possible that these changes reflect some correlations between the ILC(I) phases and the WMAP I foregrounds. The comparison between synchrotron phases for the K band shows that from Eq.(16) one can obtain $\xi_{2,2}^I - \xi_{2,1}^{III} \simeq 2.31907$ radians, while $\Phi_{2,1}^I - \Phi_{2,2}^I \simeq 2.34936$ radians. So, with accuracy about 0.030 radian we get : $\xi_{2,1}^{III} \simeq \xi_{2,2}^I - (\Phi_{2,1}^I - \Phi_{2,2}^I)$. On the other hand, from Eq.(16) one can get $\xi_{2,1}^{III} \simeq 2\xi_{2,1}^I - \xi_{2,2}^I$. Finally, combining these two equations we get:

$$2\xi_{2,1}^I + \Phi_{2,1}^I \simeq 2\xi_{2,2}^I + \Phi_{2,2}^I \quad (17)$$

As for the WMAP III, one can see that the phases of the ILC(I) and the WMAP I foregrounds per K band are strongly coupled in the form of Eq.(17). However, note that the Eq.(17), like the Eq.(11), is ‘‘empirical’’, displaying possible relationship between the phases of the ILC and the foregrounds, which requires explanation in the framework of the CMB and foreground separation scheme.

Implemented in this section phase approach can be reformulate in terms of standard correlation between different components of quadrupoles. Since the quadrupole component of the signals (the CMB and the foregrounds) contain only $a_{2,1}$ and $a_{2,2}$, the coefficient of the cross-correlation between them is simply

$$K_{1,2}^{ILC} = \frac{|a_{2,1}||a_{2,2}|\cos(\xi_{2,1} - \xi_{2,2})}{\sqrt{|a_{2,1}|^2|a_{2,2}|^2}} = \cos(\xi_{2,1} - \xi_{2,2}) \quad (18)$$

Even if the ILC quadrupole is of Gaussian nature, for a single realization of the random process, as our Universe does, this cross-correlation coefficients are not informative apart from some peculiar values such as 0 or 1. However, combining the coefficient $K_{1,2}^{ILC}$ with the same coefficient $K_{1,2}^f$, defined for the WMAP foregrounds by simple comparison between these two numbers we can conclude about common morphology of these signals.

5.2. Primordial origin ?

As is mentioned in Introduction, starting from the COBE experiment, the properties of the CMB quadrupole and particularly, the deficit of its power in comparison with the WMAP best-fit Λ CDM cosmological model has attraction of serious attention. Described in the previous section, phase correlation between the ILC and foregrounds contain important information beyond the power spectrum, providing significant restrictions on modification of the theories of inflation. From our analysis it is clear that models of inflation based on primordial Gaussian fluctuations of the inflaton field can not explain the phase correlations. Moreover, the question is if these cross-correlations can be explained in the framework of widely discussed

the Bianchi VIIIh anisotropic cosmological model (see, e.g. Refs. 24, 39 25) as this model predicts specific properties of the phases for the CMB quadrupole ? To answer this question we extract the quadrupoles of the maps derived in Refs. 39 and 25. In Fig.6 we plot both CMB maps for the range of multipoles $\ell \leq 10$ and their corresponding quadrupole components. It can be seen clearly that morphology of these quadrupoles is different from that of the ILC(III) quadrupole (see Fig.1).

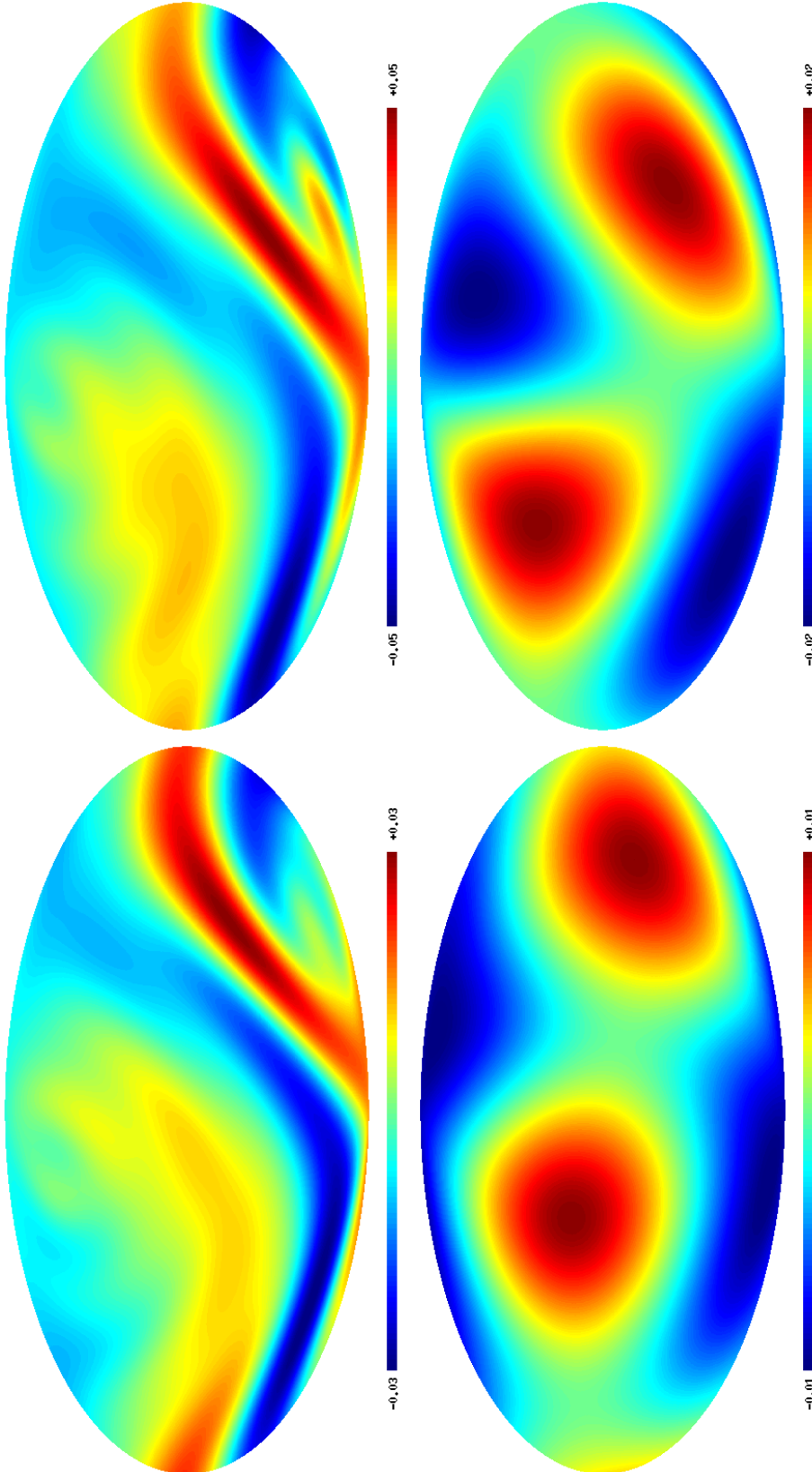
To characterize this difference, in Fig.7 we plot the phase diagram for the quadrupole modes of the ILC(III) and those from the above maps.

In spite of differences in phases between the ILC(III) and both Bianchi VIIIh quadrupoles, they have remarkable correlations. Namely, the phase difference for the ILC(III) phases is $\Delta_{III} = \xi_{2,2} - \xi_{2,1} \simeq 2.477$ rad, while for Ref. 39 quadrupole it is $\Delta_J = \xi_{2,2}^J - \xi_{2,1}^J \simeq 2.537$ radians and for Bridges et al. (2006) quadrupole it is $\Delta_B = \xi_{2,2}^B - \xi_{2,1}^B \simeq 2.560$ radians. As one can see, with error about 0.07 radians these angles Δ_{III} , Δ_J and Δ_B are the same, which means that by simple rotation of the phases we can get the same morphology of the maps. In particular, by rotation of the Ref. 39 quadrupole phases by the angle $\beta_J = 0.367$ radians counter-clockwise and by rotation of Bridges et al. (Ref. 25) phases by the angle $\beta_B = 0.317$ radians clockwise we get the ILC(III) phases with above-mentioned accuracy.

In Fig.8 we plot the difference between the Bridges et al. quadrupole (Ref. 25) after rotation of phase by the angle $\beta_B = 0.317$ radians and the ILC(III) quadrupole. Note that the peak to peak amplitude of the maps shown in Fig.8 are at the same range as the ILC(III) quadrupole: at $-200, 200\mu\text{K}$. That means that in spite of correction of the phases for Bridges et al. quadrupole (Ref. 25), the amplitudes of $a_{2,0} \div a_{2,2}$ modes still are not optimal in comparison with the ILC(III) amplitudes.

6. Conclusion

We have presented the phase analysis of the ILC(I), ILC(III) and de Oliveira-Costa and Tegmark (Ref. 35) quadrupoles in comparison with the foreground phases. We have shown that the ILC(III) quadrupole has strong correlation with the foreground phases, mainly with the synchrotron emission per K and KA band foregrounds. We have checked out the possibility that the WMAP third year data release quadrupole can be explained by implementation of the Bianchi VIIIh model discussed in Refs. 39 and 25. All these models need additional corrections of the phases for $a_{2,1}$ and $a_{2,2}$ components in order to match the phases of the ILC(III). By analysis of the de Oliveira-Costa and Tegmark (Ref. 35) quadrupoles related with a different Galactic mask we can conclude that detected above correlations between the ILC and foregrounds weakly depend on the type of the mask, if the area covered by them is small in comparison with the 4π . We have shown that transition from the ILC(I) quadrupole to the ILC(III) changes significantly the properties of the CMB-foreground phase correlations through renormalization of the gain factor. We believe that this is the main reason for discussed above phase correlation, clearly demonstrated importance of accurate removal of the systematic effects.



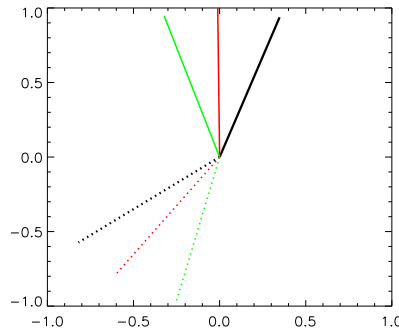


Fig. 7. Phases of the quadrupole modes of the ILC(III) and the Bianchi VIII model. The phase is represented by the angle subtended between the positive x axis and the line. Solid lines are for $(\ell, m) = (2, 1)$ modes and dotted lines for $(2, 2)$. Red lines are for ILC(III), black for Jaffe et al. and green for Bridges et al.

Acknowledgments

We thank L.-Y. Chiang, Peter Coles and Carlo Burigana for useful discussions. We acknowledge the use of the Legacy Archive for Microwave Background Data Analysis (LAMBDA). We also acknowledge the use of HEALPIX package (Ref. 40) to produce $a_{\ell m}$ and C. Copi, D. Huterer, D. Schwarz and G. Starkman for assistance in use their multipole vector package and data. OVV thanks RFBR for partly supporting by the grant No 05-07-90139. The GLESP package (Ref. 41) was used in this work.

References

1. C. L. Bennett et al., ApJS **148**, 1 (2003)
2. C. L. Bennett et al., ApJS **148**, 97 (2003), astro-ph/0203208
3. G. Hinshaw et al., ApJS **148**, 63 (2003)
4. G. Hinshaw et al., ApJS **148**, 135 (2003)
5. L.-Y. Chiang, P. D. Naselsky, O. V. Verkhodanov, P. D. Way, ApJ **590**, L65 (2003), astro-ph/0303643
6. C.-G. Park MNRAS **349**, 313 (2004), astro-ph/0307469
7. E. Martinez-Gonzalez, J. M. Diego, P. Vielva, J. Silk, MNRAS **345**, 110 (2003), astro-ph/0302094
8. H. K. Eriksen, A. J. Banday, K. M. Górski, P. B. Lilje, ApJ **612**, 633 (2004), astro-ph/0403098
9. F. K. Hansen, P. Cabella, D. Marinucci, N. Vittorio, ApJ **697**, 67L (2004), astro-ph/0402396
10. D. L. Larson, B. D. Wandelt, ApJ **613**, 85L (2004), astro-ph/0404037
11. K. Land, J. Magueijo, MNRAS **357**, 994 (2005), astro-ph/0405519
12. B. F. Roukema, B. Lew, B. Cechowska, A. Marecki, S. Bajtlik, A&A **423**, 825 (2004), astro-ph/0402608
13. C. J. Copi, D. Huterer, G. D. Starkman, Phys. Rev. D **70**, 043515 (2004), astro-ph/0310511
14. G. Chen et al., ApJ **611**, 655 (2004), astro-ph/0403695

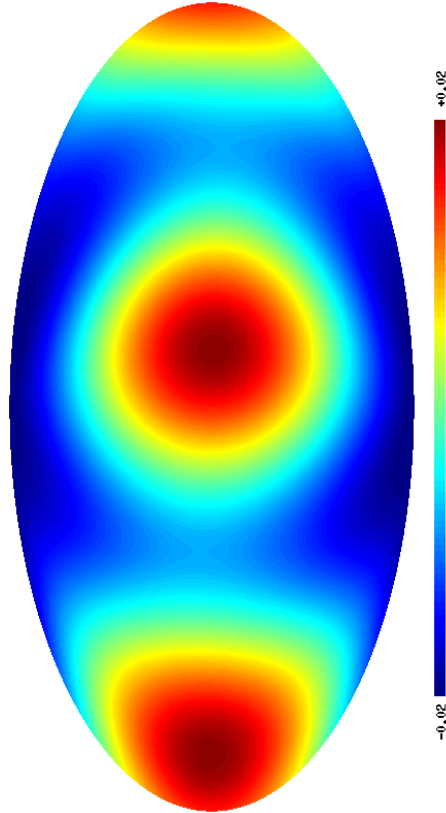


Fig. 8. The map for difference between corrected by the angle β_B Bridges et al. quadrupole and the ILC(III).

15. J. D. McEwen, M. P. Hobson, A. N. Lasenby, D. J. Mortlock, MNRAS **359**, 1583 (2005), astro-ph/0406604
16. T. R. Jaffe et al., ApJ **629**, 1 (2005), astro-ph/0503213
17. P. D. Naselsky, A. G. Doroshkevich, O. V. Verkhodanov, MNRAS **349**, 695 (2004), astro-ph/0310601
18. L.-Y. Chiang, P. D. Naselsky, To appear in Int. J. Mod. Phys. D, astro-ph/0407395
19. P. Dineen, P. Coles MNRAS **347**, 52 (2004), astro-ph/0306529
20. D. N. Spergel et al., Submitted to ApJ, astro-ph/0603449
21. G. Hinshaw et al., Submitted to ApJ, astro-ph/0603451
22. D. J. Schwarz, G. D. Starkman, D. Huterer, C. J. Copi Phys. Rev. Lett. **93**, 221301 (2004), astro-ph/0403353
23. C. J. Copi, D. Huterer, D. Swartz, G. D. Starkman, astro-ph/0605135
24. T. R. Jaffe et al., ApJ **644**, 701 (2006), astro-ph/0512433
25. M. Bridges, J. D. McEwen, A. N. Lasenby, M. P. Hobson, Submitted to MNRAS, astro-ph/0507186
26. R. C. Helling, P. Schupp, T. Tesileanu, astro-ph/0603594
27. M. Tegmark, A. de Oliveira-Costa, Phys. Rev. D **68**, 123523 (2004), astro-ph/03022496
28. P. D. Naselsky, A. G. Doroshkevich, O. V. Verkhodanov, ApJ **599**, 53 (2003), astro-

- ph/0310542
29. P. D. Naselsky, I. D. Novikov, L.-Y. Chiang, *ApJ* **642**, 617 (2006), astro-ph/0506466
 30. P. Bielewicz et al., *ApJ* **635**, 750 (2005), astro-ph/0507186
 31. L.-Y. Chiang, P. D. Naselsky, P. Coles, Submitted to *ApJL*, astro-ph/0603662
 32. M. Cruz et al., Submitted to *ApJ*, astro-ph/0603859
 33. P. E. Freeman, C. R. Genovese, C. J. Miller, R. C. Nichol, L. Wasserman, *ApJ* **638**, 1 (2006), astro-ph/0510406
 34. R. D. Blandford, *Measuring and Modeling the Universe: A Theoretical Perspective* Measuring and Modeling the Universe, from the Carnegie Observatories Centennial Symposia. (Carnegie Observatories Astrophys. Ser., 2004) p.377
 35. A. de Oliveira-Costa, M. Tegmark, *Phys. Rev. D* **74**, 023005 (2006), astro-ph/0603369
 36. L.-Y. Chiang, *MNRAS* **325**, 405 (2001), astro-ph/0011021
 37. L.-Y. Chiang, *MNRAS* **350**, 1310 (2004), astro-ph/0309323
 38. T. Matsubara, *ApJ* **591**, L79 (2003), astro-ph/0303278
 39. T. R. Jaffe et al., Submitted to *A&A Research Note*, astro-ph/0606046
 40. K. M. Górski et al., *ApJ* **622**, 759 (2005), astro-ph/0409513
 41. A. G. Doroshkevich et al., *Int. J. Mod. Phys. D* **14**, 275 (2005), astro-ph/0305537

